JMB

Structure, Dynamics and Thermodynamics of the Human Centrin 2/hSfi1 Complex

Juan Martinez-Sanz[1,2]**, Fatiha Kateb**[3]**, Liliane Assairi**[1,2]**, Yves Blouquit**[1,2]**, Geoffrey Bodenhausen**[3]**, Daniel Abergel**[3]**, Liliane Mouawad**[1,2]***** and Constantin T. Craescu**[1,2]†

[1]*Institut Curie–Centre de Recherche, F-91405 Orsay Cedex, France*

[2]*Institut National de la Santé et de la Recherche Médicale (INSERM) U759, F-91405 Orsay Cedex, France*

[3]*Département de Chimie, Associé au Centre National de la Recherche Scientifique, Ecole Normale Supérieure, 24 rue Lhomond, 75231 Paris Cedex 05, France*

Received 17 July 2009; received in revised form 16 October 2009; accepted 17 October 2009
Available online 24 October 2009

Centrin, an EF-hand calcium-binding protein, has been shown to be involved in the duplication of centrosomes, and Sfi1 (Suppressor of fermentation-induced loss of stress resistance protein 1) is one of its centrosomal targets. There are three isoforms of human centrin, but here we only considered centrin 2 (HsCen2). This protein has the ability to bind to any of the ~25 repeats of human Sfi1 (hSfi1) with more or less affinity. In this study, we mainly focused on the 17th repeat (R17-hSfi1-20), which presents the highest level of similarity with a well-studied 17-residue peptide (P17-XPC) from human xeroderma pigmentosum complementation group C protein, another centrin target for DNA repair. The only known structure of HsCen2 was resolved in complex with P17-XPC. The 20-residue peptide R17-hSfi1-20 exhibits the motif L8L4W1, which is the reverse of the XPC motif, W1L4L8. Consequently, the dipole of the helix formed by this motif has a reverse orientation. We wished to ascertain the impact of this reversal on the structure, dynamics and affinity of centrin. To address this question, we determined the structure of C-HsCen2 [the C-terminal domain of HsCen2 (T94–Y172)] in complex with R17-hSfi1-20 and monitored its dynamics by NMR, after having verified that the N-terminal domain of HsCen2 does not interact with the peptide. The structure shows that the binding mode is similar to that of P17-XPC. However, we observed a 2-Å translation of the R17-hSfi1-20 helix along its axis, inducing less anchorage in the protein and the disruption of a hydrogen bond between a tryptophan residue in the peptide and a well-conserved nearby glutamate in C-HsCen2. NMR dynamic studies of the complex strongly suggested the existence of an unusual calcium secondary binding mode in calcium-binding loop III, made possible by the uncommon residue composition of this loop. The secondary metal site is only populated at high calcium concentration and depends on the type of bound ligand.

© 2009 Elsevier Ltd. All rights reserved.

Edited by M. F. Summers

Corresponding author. Imagerie Integrative, Institut Curie–Centre de Recherche/INSERM U759, Centre Universitaire d'Orsay, Bâtiment 112, F-91405 Orsay Cedex, France. E-mail address: Liliane.Mouawad@curie.u-psud.fr.

† Deceased.

Introduction

Centrins are acidic Ca^{2+}-binding proteins from the EF-hand superfamily that are well conserved in the eukaryotic realm.[1,2] These small proteins ($\sim$ 20 kDa) are composed of two relatively independent EF-hand domains. Each domain consists of two EF-hand motifs and possesses two potential Ca^{2+}-binding sites with varying affinities that are determined largely by the amino acid sequence of the binding loops.

Centrins were first identified in unicellular green algae, such as *Tetraselmis striata*[3] and *Chlamydomonas reinhardtii*,[4,5] as components of the contracting fibers associated with the basal bodies. In these organisms, the centrin-containing fibers form a continuous filamentous scaffold extending from the nucleus–basal body connector to the distal contractile fibers.[6] The capacity of the centrin-based filaments to contract upon increased Ca^{2+} concentration, even in the absence of ATP,[3] suggests that centrins are responsible for calcium-dependent motility, at least in ciliated or flagellate cells. Flagellar excision, as a response to adverse environmental conditions in algae, is also dependent on centrin filaments and seems to be regulated by the cellular Ca^{2+} concentration.[5]

Centrins have since been found to be ubiquitous proteins in many other eukaryotic species, including higher plants,[7] yeasts,[8] invertebrates[9] and humans[10,11] (see the work of Wolfrum *et al.*[12] for a review). A small fraction of centrins are concentrated in the microtubule organizer centers, which are structurally and functionally similar to basal bodies and are known as the spindle pole bodies in yeast and as the centrosome in higher eukaryotes. It was clearly demonstrated in several eukaryotic species that when centrin is absent or non-functional, microtubule organizer center duplication is blocked and cellular mitosis is seriously perturbed.[13–17] However, the role of centrins in cell cycle regulation is not yet known.

Additional implications of centrins in other cellular processes, including nucleotide excision repair,[18] the light transduction cascade in photoreceptor cells,[19] the ciliary voltage-gated Ca^{2+} channel in *Paramecium*,[20] axonemal chemotaxis in *Tetrahymena*[21] and the nuclear mRNA export machinery in yeast,[22] have been recently observed. The role of calcium in the regulation of these functions has not yet been clearly established.

Significant progress in the understanding of the centrosomal function of centrins was achieved with the discovery of the centrin target Sfi1 (Suppressor of fermentation-induced loss of stress resistance protein 1), a large protein containing 24 (or 25, see below) repeated sequence motifs, each of which can bind a centrin molecule.[23] Previous centrin/ Sfi1 interaction studies[24] showed that the binding affinity is moderately dependent on Ca^{2+} concentration, suggesting that the two proteins are bound constitutively.

Two crystal structures of the integral centrin are presently available: human centrin 2 (HsCen2) in complex with a 17-residue peptide derived from the human xeroderma pigmentosum complementation group C protein (XPC) [P17-XPC (peptide N847–R863 from the human XPC protein)][25,26] and yeast (*Saccharomyces cerevisiae*) Cdc31 in complex with two or three repeats of ScSfi1.[27] The global shape of the domains is similar for the two centrins: the N-terminal domain is in a closed conformation, where the helices of the EF hand are anti-parallel, whereas the C-terminal domain is in an open conformation, with perpendicular helices. Contrary to calmodulin (CaM) and troponin C, the C-terminal domain of these centrins prefers to adopt the open conformation in the absence of Ca^{2+}.[28,29] Consequently, HsCen2 and Cdc31 may bind their targets constitutively through a deep hydrophobic cavity of the C-terminal domain.

The differences between these two complexes may arise from either the centrin itself or from its target. While the conformations of the N- and C-terminal domains of these centrins are very similar, the difference arises in the interdomain linker around Pro94 of Cdc31, which is well conserved only in the Cdc31 centrin subfamily. Indeed, HsCen2 is an extended dumbbell-shaped protein ([Fig. 1]) in which the linker between the two domains consists of one straight helix as in unbound holo-CaM,[30] whereas in Cdc31 the linker is bent due to the presence of this proline. The linker bending of Cdc31 brings the N-terminal domain in contact with the N-terminal moiety of the ScSfi1 repeat. These contacts were proposed to be important for the stabilization of the complex.[27] Here, we asked whether these interactions are merely a consequence of the Pro-bent linker of Cdc31 (and are therefore specific to this centrin subfamily) or whether they are a feature of other centrin subfamilies, such as *C. reinhardtii* centrin (that includes HsCen2).

In XPC, the interacting part of the peptide forms a helix with the sequence motif Wx_2Lx_3L (also denoted W1L4L8), which is strongly conserved in this protein in various organisms; in some Sfi1 repeats, the corresponding motif is Lx_3Lx_2W. Herein, we denote Lx_3Lx_2W as L8L4W1 for convenience (in most cases, L4 is replaced by other hydrophobic residues, and in some repeats, L8 is replaced by polar or charged residues). Since the Trp residue occupies the same cavity in both complexes, this sequence inversion corresponds to a reversed orientation of the target helices and consequently to an inversion of the helix dipole. Therefore, we may ask how HsCen2 accommodates this dipole inversion, knowing that the negative end of the peptide helix will interact with a more negatively charged region in HsCen2 than in Cdc31 (there are six acidic residues in HsCen2 and five acidic residues plus one basic residue in Cdc31 in the neighboring G-helix). What would be the structural, thermodynamic and dynamic consequences of this inversion?

In order to answer these questions, we performed structural and dynamic NMR studies of C-HsCen2 [the C-terminal domain of HsCen2 (T94–Y172)] in complex with a human Sfi1 (hSfi1) repeat [peptide R641–T660 of the human Sfi1 (R17-hSfi1-20)] that
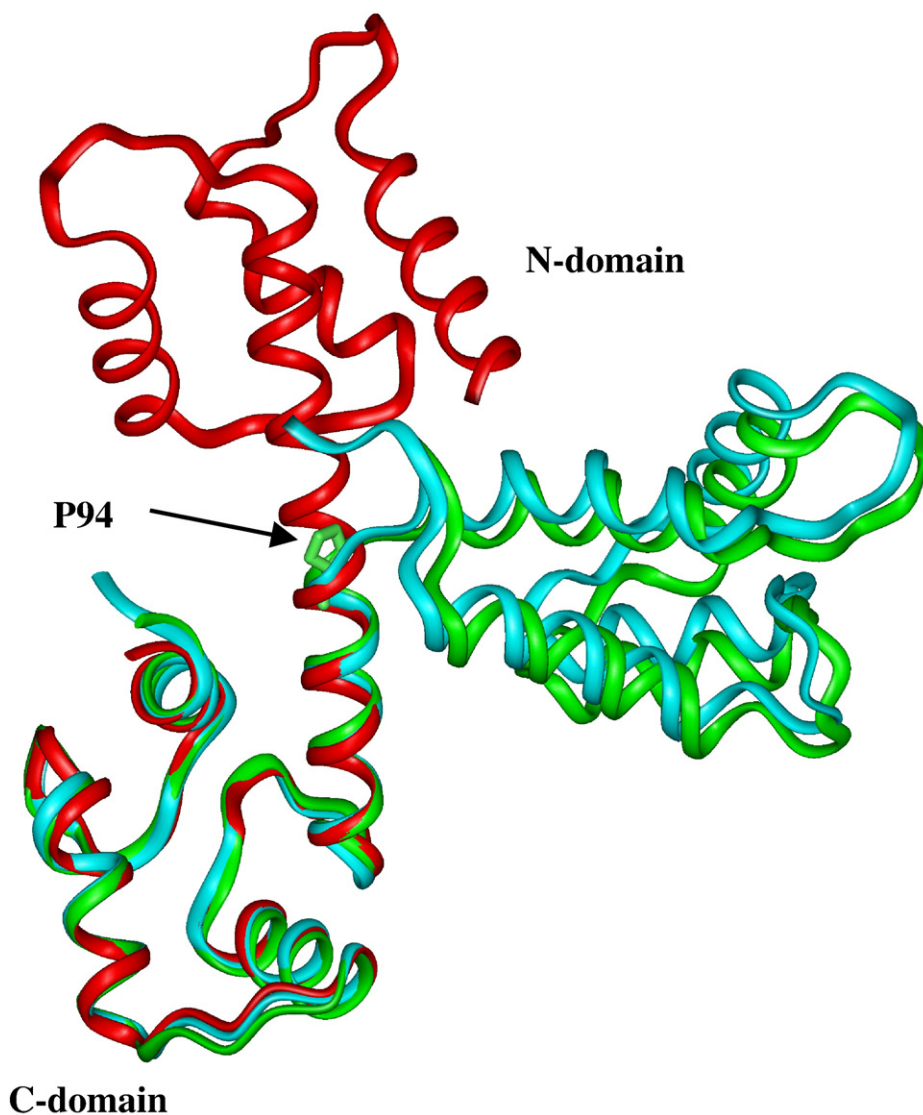
Fig. 1. Superposition of the crystal structures of HsCen2 in complex with P17-XPC (PDB code 2OBH, red) and of Cdc31 bound to an ScSfi1 repeat in the presence (PDB code 2DOQ, in green) and that in the absence (PDB code 2GV5, in cyan) of Ca^{2+}. The backbones of the C-terminal domains were superimposed. The position of Pro94 in Cdc31 is indicated.

contains the triad L8L4W1 and used isothermal titration calorimetry (ITC) to explore the thermodynamic properties of the interaction of HsCen2 with various hSfi1 repeats.

Results and Discussion

Three of the 24 identified repeats of hSfi1 (i.e., R17, R18 and R21) contain the triad L8L4W1. The 17th repeat (R17), encompassing residues 641–660 of hSfi1, was chosen for structural and dynamic studies because, in addition to the triad, it contains an Ala residue in the fifth position with respect to W1, as in the peptide P17-XPC. In the complex HsCen2/P17-XPC, the corresponding alanine interacts with Phe113 of HsCen2 (see the structural description below). Furthermore, in the extension of this repeat, there is another Ala that is believed to interact with

N-HsCen2 [the N-terminal domain of HsCen2 (M1–S98)] as in the yeast complex (Fig. 2). Indeed, the crystal structure of Cdc31/ScSfi1[27] revealed the presence of some contacts between the N-terminal domain of the centrin and residues from the N-terminal moiety of the repeats, in particular alanine (A17) in position 17 upstream from the conserved Trp. In this position, there are an Ala in 47% of the yeast repeats and in 80% of the human repeats. However, several other constructs were also considered in thermodynamic studies (Fig. 2).

Thermodynamic analyses of interactions between centrin 2 and hSfi1 repeats

The interaction of the R17-hSfi1-20 peptide (where 20 refers to the length of the peptide) with HsCen2 in the presence or absence of Ca^{2+} showed by ITC, as in previous studies,[24] that the binding

(a)

	`- 17- - - - - - 10- 8 - - 5 4 - - 1 --`
R17-hSfi1-20 (641–660)	RADLHHQHSVLHRALQAWVT
R17-hSfi1-12 (649–660)	SVLHRALQAWVT
R17-hSfi1-6 (655–660)	LQAWVT
R0-hSfi1-20 (81–100)	GRLRELRIRSVARKFLYLWI
R9-hSfi1-20 (374–393)	EMAEEHHRHSQLYFCFRALK
R18-ScSfi1-20 (680–699)	IQAISKRNYQLEKMVLKKFR

(b)

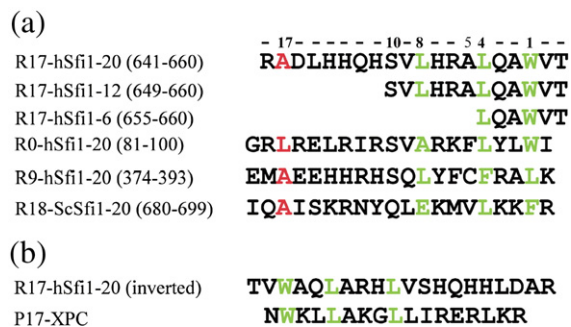|	
R17-hSfi1-20 (inverted)	TVWAQLARHLVSHQHHLDAR
P17-XPC	NWKLLAKGLLIRERLKR

Fig. 2. (a) Amino acid sequences of the peptides used in the present work. Residues in green represent the hydrophobic triad responsible for the interaction with centrin. Residues in red occupy the same position (the 17th position upstream from the tryptophan of the triad) as the alanine that was described to interact with the N-terminal domain of Cdc31. The Cys in position 10 was replaced by a Ser in the R0-hSfi1-20 peptide (see Materials and Methods). (b) Alignment of the reversed R17-hSfi1-20 sequence with the sequence of P17-XPC showing the common hydrophobic triad (green) in XPC and hSfi1 peptides.

affinity is only weakly dependent on Ca^{2+} concentration, suggesting that HsCen2 and R17-hSfi1 interact constitutively (Table 1). To examine the importance of the interaction between N-HsCen2 (M1-S98) and the peptide, we measured separately the affinity of each domain of HsCen2 for R17-hSfi1-20. In addition, we measured the affinity of the integral HsCen2 for a truncated repeat of 12 residues, R17-hSfi1-12, in which A17 is absent. The results (Table 1) do not show any measurable interaction between N-HsCen2 (residues 1–98) and R17-hSfi1-20, while they showed similar affinities for the C-HsCen2/R17-hSfi1-20, HsCen2/R17-hSfi1-20 and HsCen2/R17-hSfi1-12 complexes, in the presence or absence of Ca^{2+}, suggesting that the HsCen2/hSfi1 interface involves only the C-terminal domain (residues 94–172) of HsCen2. This observation raised the question of the minimal binding sequence within an Sfi1 repeat. A peptide representing only

the last six residues of the R17 repeat (R17-hSfi1-6) showed no detectable binding to HsCen2, indicating that the complete hydrophobic triad LLW is necessary for the interaction to be significant.

In the R9-hSfi1-20 peptide, a leucine occurs instead of W1 (Fig. 2). ITC experiments on HsCen2/R9-hSfi1-20 were used to evaluate the consequences of this substitution. Because of the lower solubility of the peptide, we performed the reverse experiment, in which the peptide is titrated by the protein. As may be seen in Fig. 3 and Table 1, the presence of a Leu residue instead of Trp has practically no effect on the binding affinity of the R9 repeat. The enthalpy of interaction is lower, probably due to the smaller number of apolar contacts between the Leu side chain and the protein. However, the observed decrease of the intermolecular forces is compensated by a more favorable entropic component, such that the free energy of binding is similar to that of the reference peptide, R17-hSfi1-20.

The protein hSfi1 was described to contain 24 repeats of 23 residues each, with neighboring repeats separated by 10 residues.[23] A careful sequence analysis of hSfi1 suggested the presence of an additional motif, which we called R0-hSfi1-20 (Fig. 2), located 6 residues upstream from the R1 repeat. The ITC experiments performed with the corresponding peptide (Fig. 3) showed that the binding affinity and the energetic balance are very similar to those observed for other canonical repeats (Table 1), confirming the hypothesis that this repeat constitutes an additional HsCen2 binding site.

In one of the yeast complexes, the crystal structure of which is known in the apo state, the repeat R18-ScSfi1 presents an infrequent triad E8L4F1 (only 2 of the 24 repeats in hSfi1 and 1 of the 21 repeats of ScSfi1 contain an acidic residue at their eighth position). In the crystal structure, the interaction Cdc31/ScSfi1 does not seem to be perturbed by this substitution. Here, ITC experiments were carried out on the complex formed by HsCen2 with this repeat from the yeast Sfi1 (Figs. 2 and 3). The results showed that the affinity of the peptide in the presence of Ca^{2+} is about 1 order of magnitude lower than the affinity of R17-

Table 1. Thermodynamic parameters of various repeats and variants of Sfi1 binding to HsCen2 in the presence or absence of 1 mM Ca^{2+}

Protein	Ca^{2+}	Ligand	K_a(±error) (10^6 M^{-1})	ΔG (kcal mol^{-1})	ΔH (±error) (kcal mol^{-1})	$T\Delta S$ (kcal mol^{-1})
HsCen2[a]	+	R17-hSfi1-20	6.5 (0.9)	−9.5	−20.3 (0.3)	−10.8
HsCen2[a]	−	R17-hSfi1-20	0.25 (0.02)	−7.5	−17.1 (0.5)	−9.6
C-HsCen2[a]	+	R17-hSfi1-20	14 (1)	−9.9	−17.7 (0.08)	−7.8
C-HsCen2[a]	−	R17-hSfi1-20	2.6 (0.2)	−8.9	−20.1 (0.2)	−11.2
N-HsCen2	+	R17-hSfi1-20	NB[b]			
HsCen2[c]	+	R9-hSfi1-20	5.5 (0.5)	−9.4	−15.2 (0.2)	−5.8
HsCen2[c]	−	R9-hSfi1-20	0.091 (0.05)	−6.9	−7.2 (0.2)	−0.3
HsCen2	+	R17-hSfi1-12	4.3 (0.4)	−9.2	−25.8 (0.3)	−16.6
HsCen2	−	R17-hSfi1-12	0.023 (0.001)	−6.1	−27.9 (1.0)	−21.8
HsCen2	+	R17-hSfi1-6	NB[b]			
HsCen2	+	R0-hSfi1-20	7.0 (0.4)	−9.5	−20.5 (0.1)	−11.0
HsCen2	+	R18-ScSfi1-20	0.48 (0.03)	−7.9	−12.9 (0.4)	−5.0

[a] From Martinez-Sanz *et al.*[24]
[b] NB indicates no binding was observed in the present conditions ($K_a < 10^4$ M^{-1}).
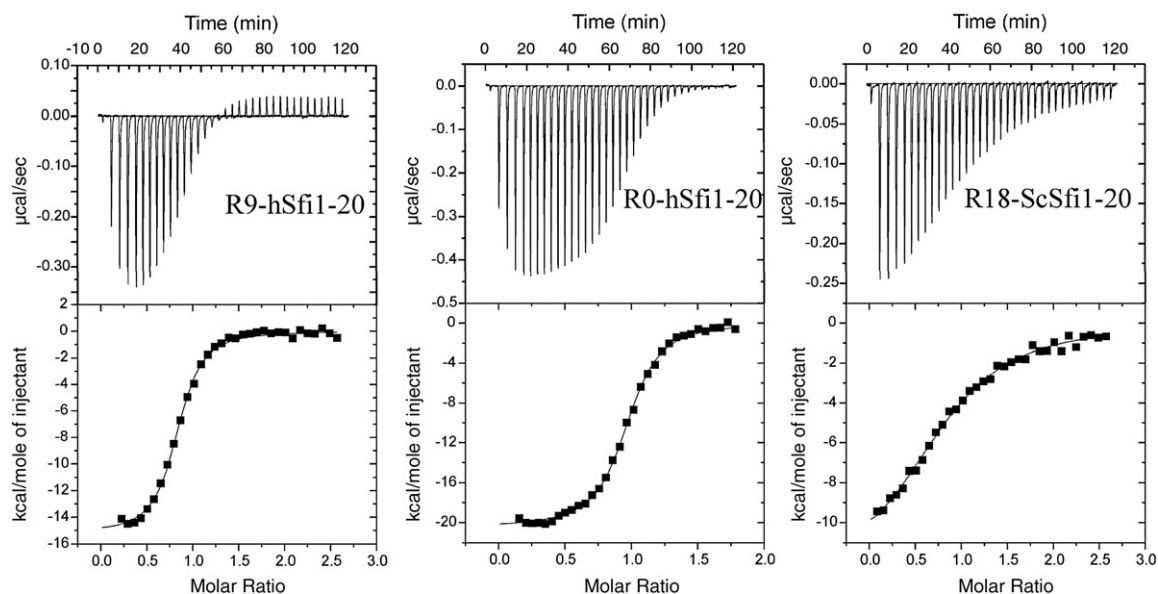[c] The peptide was titrated by the protein in these experiments.

Fig. 3. ITC measurements of HsCen2 with two repeats from hSfi1 and one repeat from ScSfi1 in the presence of 1 mM Ca^{2+}. The upper panels show the raw data, and the lower panels show the binding isotherms fitted to a single-site binding model.

hSfi1-20 (Table 1). Therefore, the difference of affinity between these two peptides in the presence of Ca^{2+} is not as drastic as the difference between R17-hSfi1-20 and R17-hSfi1-6, with the latter lacking the residue in the eighth position of the triad.

Ca^{2+} dependence

The ITC measurements show that the affinity of HsCen2 for hSfi1 repeats decreases by 1 or 2 orders of magnitude in the absence of Ca^{2+}. The same Ca^{2+} dependence was previously observed for XPC.[31] This moderate Ca^{2+} sensitivity seems to be specific to centrin interactions[31,32] with regard to the calcium-sensor proteins. It stands in contrast to the case of CaM,[33] which exhibits a much stronger Ca^{2+} dependence for a broad range of targets. The weak Ca^{2+} dependence of the centrin interactions can be related to the unusually low stability of the closed conformation of the apo C-terminal domain.[29,34] In the absence of Ca^{2+}, a significant fraction of molecules adopt an open conformation and are able to bind the target peptide.

Assessing the interaction centrin 2/R17-hSfi1-20 by NMR

ITC measurements have shown that both the integral HsCen2 and its C-terminal domain bind the hSfi1 repeats with very similar free energies, suggesting that only the C-terminal domain is significantly involved in the interaction. This hypothesis was further supported by the analysis of the NMR spectra of centrin 2 uniformly labeled with ^{15}N in complex with R17-hSfi1-20. Figure S1a shows a superposition of the heteronuclear single-quantum coherence (HSQC) spectra corresponding to the peptide-bound forms of the integral centrin and of the isolated C-terminal domain, as well as the unbound form of the N-terminal domain. The cross-peaks of the integral protein complex are significantly broader because of the larger molecular mass, while the signals of the peptide-free N-terminal domain superpose quite well with a subclass of peaks of the complex formed by the integral protein. The few observed discrepancies are due to the N- and C-termini of the isolated domain, which are very flexible. Notably, the C-terminus of the N-terminal domain in the integral protein is a well-structured α-helix, while it is unstructured in the isolated domain. In addition, a detailed analysis of the three-dimensional NMR spectra, including sequential assignments, revealed a high level of similarity between the spectral features of the N-terminal domain, either alone or as a part of the integral protein. These observations indicate that this domain does not interact significantly with the hSfi1 repeat R17. This raised the question of the mode of action of HsCen2 on hSfi1. It was proposed in the yeast spindle pole body that centrin proteins decorate ScSfi1 and that they may induce contractions of the Sfi1 fiber upon Ca^{2+} addition.[27] This model cannot be directly applied to the human centrosome because of the differences between the HsCen2/hSfi1 and Cdc31/ScSfi1 complexes. In the human case, either HsCen2 proteins decorate hSfi1 and induce fiber contractions in a different way (see the model proposed by Martinez-Sanz *et al.*[24]) or the natural target of hSfi1 is HsCen3, another human centrin isoform belonging to the Cdc31 subfamily, in which case it decorates hSfi1 in a way similar to that of the yeast complex.

The peaks corresponding to the isolated C-terminal domain in the complex with R17-hSfi1-20 also nicely superpose onto a subclass of peaks of the

complex formed by the integral protein. Therefore, linking the halves of the protein together maintains the conformational features of each half, which is consistent with a high degree of structural autonomy. For these reasons, we decided to limit our structural study to the C-terminal domain complex.

Structural description of the C-HsCen2/R17-hSfi1-20 complex

We have shown that the binding affinity of R17-hSfi1-20 to HsCen2 increases by 1 order of magnitude in the presence of Ca^{2+}. There are four calcium-binding loops in HsCen2; in the N-terminal domain, loops I and II do not bind Ca^{2+} at physiological concentrations, while loop III (D114–N125) and loop IV (D150–E161) bind Ca^{2+} with moderate affinity ($\sim 10^4$ M^{-1}) and more strongly ($\sim 10^5$ M^{-1}), respectively. Preliminary Ca^{2+} titration experiments showed that only the binding of the first Ca^{2+} ion to high-affinity site IV is necessary to stabilize the complex. Addition of further Ca^{2+} ions leads to severe line broadening of several peaks corresponding to residues in site III. The solution structure of the C-HsCen2/R17-hSfi1-20 complex was therefore determined in the presence of only one Ca^{2+} equivalent. The ^{15}N–^{1}H HSQC spectrum (Fig. S1b) indicates that the complex has a well-determined, unique structure. The assignments could be completed for the ^{1}H, ^{15}N and ^{13}C resonances corresponding to residues 100–169, while the flexible terminal residues 94–99 and residues 170–172 remain unassigned. One- and two-dimensional ^{15}N- and ^{13}C-filtered spectra were used for the assignment of the resonances of the R17-hSfi1-20 peptide.[35] Overall, 1339 distance and angle restraints, including 71 intermolecular restraints, were used for simulated annealing (Table 2). The small RMSD values of the final 15 NMR structures

and the absence of significant violations indicate the quality of these structures. Analysis of the calculated structures by PROCHECK-NMR shows that 95.5% of the backbone dihedral angles are distributed in the allowed regions of Ramachandran plots. The residues lying in the generously allowed or disallowed regions of the plots are located in the N- and C-termini of the domain, as well as in its loops. The 15 best structures of the complex were deposited in the Protein Data Bank (PDB) under accession code 2K2I. A stereoview of these structures, in which the backbones of the helices are superimposed, is represented in Fig. 4a. The figure shows that C-HsCen2 in the complex adopts the classic structure of a Ca^{2+}-saturated EF-hand domain, with the two EF-hand motifs coupled through an anti-parallel β-strand. Some structural disorder, arising from a lack of experimental restraints, may be noted in the N-terminal (94–99) and C-terminal (169–172) parts of the C-HsCen2 domain, as well as in the linker between the two EF-hand motifs and in the nine N-terminal residues of the hSfi1 peptide. In contrast, the α-helices (E: K101–F113, F: F124–E132, G: D142–A149, H: E159–K168) and the β-strands (β3: K120–S122, β4: E156–S158) are well defined. The mean interhelical angles in the two EF-hand motifs of C-HsCen2, calculated with the Interhlx software (K. Yap, University of Toronto, Toronto, Canada), are E/F = 93.0° ± 4.3° and G/H = 95.3° ± 3.7°, which fall into the typical range of values observed for open EF-hand domains. This open conformation creates a deep hydrophobic cavity divided into two parts by the side chain of Phe113 and bordered mostly by negatively charged side chains (Fig. 4b).

Consequences of the helix dipole orientation

In the complex, the R17-hSfi1-20 peptide partially folds into an α-helix that spans the fragment L651–

Table 2. Restraint and structural statistics for the 15 best solution structures of the C-HsCen2/R17-hSfi1-20 complex

|	
Restraint statistics	
Intramolecular NOE restraints	1064
Intraresidue	287 (27%)
Sequential	326 (31%)
Medium range ($2 \leq |i-j| < 5$)	269 (25%)
Long range ($|i-j| \geq 5$)	182 (17%)
Hydrogen-bond restraints	84
Dihedral angle restraints (Φ,Ψ)	120
Intermolecular NOE restraints	71
Average number of restraint violations	
Violations per structure (>0.5 Å)	None
Dihedral angle restraint violations (>10°)	None
RMSD for covalent bonds relative to standard	0.024 Å
RMSD for covalent angles relative to standard	2.7°
Average RMSD (Å) from the average structure	
Helices E, F, G and H and β-sheet[a]	0.62
Helices E, F, G and H and β-sheet, peptide 641–660[a]	0.66
All atoms in protein residues 102–168 and peptide 641–660	0.86
Ensemble Ramachandran plot	
Residues in the most favored region	79.8%
Residues in additionally allowed regions	15.7%
Residues in generously allowed regions	3.0%
Residues in disallowed regions	1.5%

[a] Backbone atoms (N, C′, Cα).
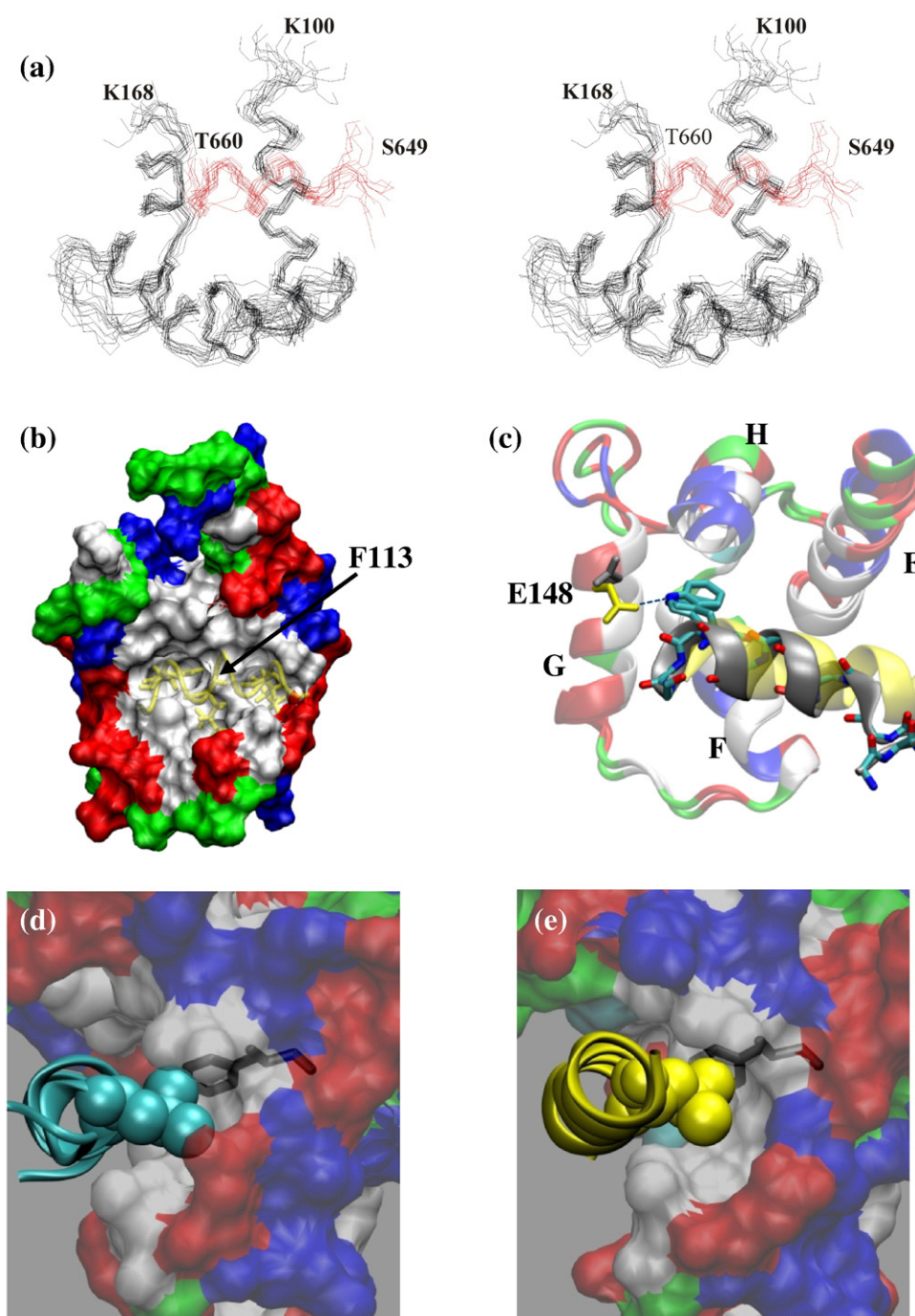
Fig. 4. Structural features of the C-HsCen2/R17-hSfi1-20 complex. (a) Stereoview of the superposition of the 15 best NMR structures obtained in this work. The centrin domain is shown in black, and the peptide is shown in red. The structure was determined for C-HsCen2 in complex with R17-hSfi1-20, but only relatively ordered structural fragments are shown. (b) The accessible surface representation of the best C-HsCen2 structure, colored according to residue type (hydrophobic, white; polar, green; basic, blue; acidic, red). Only the structured part of the peptide is shown in transparent yellow. It can be seen that the binding site consists of two deep hydrophobic cavities separated by F113. (c) Superposition of the backbones of C-HsCen2 in complex with R17-hSfi1-20 and that with P17-XPC (PDB code 2GGM). The color code of the C-terminal domain is the same as that in (b). In the C-HsCen2/P17-XPC structure, residue E148 and the peptide are shown in yellow. In the C-HsCen2/R17-hSfi1-20 structure, E148 and the peptide are in gray. In addition, in the latter case, the backbone of the peptide is drawn with the following color code: carbon atoms in cyan, nitrogens in blue and oxygens in red. The carbonyl groups of the hSfi1 peptide indicate the orientation of the helix dipole. The Trp side chain is shown in both structures. Panels (d) and (e) represent comparisons of the C-HsCen2/R17-hSfi1-20 and HsCen2/P17-XPC complexes, respectively. Residue F113 (black sticks) of C-HsCen2 interacts less strongly with L8 of hSfi1 [cyan spheres in (d)] than L8 of XPC [yellow spheres in (e)]. In both (d) and (e), the target peptide is shown as a ribbon and the color code of the accessible surface of the fragment of C-HsCen2 is the same as in (b).

T660. As mentioned above, the helix dipole of this peptide is reversed with respect to that of P17-XPC. However, the tryptophan side chains of both peptides are similarly embedded in the cavity of HsCen2, which comprises residues F113, I121, L126, M145, I146, E148, A149, V157, F162 and I165. For hSfi1, this implies a rotation of the Trp side chain (the χ_1 dihedral torsion angle, defined by the atoms N, C^α, C^β and C^γ, is around $-80°$ in XPC and is about $-160°$ in hSfi1) and a slight translation (~ 2 Å) of the peptide helix along its axis toward the HsCen2 G-helix and more specifically E148 (Fig. 4c). Our observations indicate that this glutamate may play a significant role in the interaction with the peptide. Indeed, in the crystal[25,26] and NMR[34] structures of the complex HsCen2/P17-XPC, the carboxyl group of E148 faces the positive pole of the peptide helix and establishes a hydrogen bond with the tryptophan of XPC (either with the $N^{\varepsilon 1}$ atom of its side chain or with the amide N of its backbone through a water molecule), whereas in the complex with R17-hSfi1, E148 faces the negative pole of the peptide helix that pushes the Glu side chain away from Trp, leading to a disruption of the H-bond. This observation is corroborated by the presence of several medium and weak nuclear Overhauser enhancement (NOE) effects between the tryptophan of P17-XPC and E148 of HsCen2, whereas no corresponding effect was observed between E148 and the tryptophan of R17-hSfi1-20 (the lists of the NMR restraints are available in the PDB, linked to structures 2A4J and 2K2I of complexes HsCen2/P17-XPC and HsCen2/R17-hSfi1-20, respectively). We observed similar relative positions between Cdc31 E140 and ScSfi1 tryptophan in the crystal structure of yeast Cdc31/ScSfi1 complexes.[27] In addition, the difference of interaction mode between the corresponding Glu and the peptide Trp with respect to the peptide dipole orientation may be observed for CaM complexes with the Ca^{2+}/CaM-dependent kinase peptide (PDB code 1IQ5) and smooth muscle myosin light chain kinase (PDB code 1CDL) that also differ by a peptide helix inversion. It is worth noting that this Glu is highly conserved in the EF-hand motifs of most centrins, CaM and troponin C (although it is replaced by an Asp in the latter). In all known structures, it is oriented toward the target peptide when the positive end of the helix dipole points to this acidic residue, whereas it is oriented outward if the position of the dipole is reversed.

In HsCen2/P17-XPC complex, it was observed that four hydrophobic residues of the target peptide (W1, L4, A5 and L8) envelop the centrin Phe113, establishing important hydrophobic contacts, whereas in the C-HsCen2/R17-hSfi1-20 complex, because of the slight translation of the peptide with respect to centrin, the contact between F113 and L8 is significantly reduced, which weakens the hydrophobic contacts (Fig. 4d and e). Therefore, despite the fact that the triad WLL (or LLW) is well conserved in XPC and R17 of hSfi1, the lack of some interactions between the latter and human centrin (E148 and F113) due to the helix dipole

inversion may account for the lower enthalpy $\Delta\Delta H(XPC-hSfi1) \approx -7$ kcal/mol and the lower free binding energy $\Delta\Delta G(XPC-hSfi1) \approx -2$ kcal/mol of this peptide.

Effects of Ca^{2+} on dynamics

The classic NMR method for studying the internal dynamics of proteins is to measure the longitudinal and transverse relaxation rates $R_1(^{15}N)$ and $R_2(^{15}N)$ of ^{15}N single-quantum coherence of amide nitrogens that provide information concerning fast (picosecond to nanosecond) and slow (microsecond to millisecond) motions of the backbone.

Fast motions

The overall tumbling of the C-HsCen2/R17-hSfi1-20 complex was assumed to be isotropic, similar to the C-HsCen2/P17-XPC complex that was investigated in a previous study.[36] The overall correlation time τ_c of the C-HsCen2/R17-hSfi1-20 was determined from $R_1(^{15}N)$ and $R_2(^{15}N)$ relaxation rates. Nearly identical values $\tau_c = 5.41 \pm 0.25$ ns and $\tau_c = 5.52 \pm 0.38$ ns were found for samples with an equimolar concentration (1 mM) and large excess (8 mM) of Ca^{2+}, respectively. These data indicate that the complex was monomeric up to 8 mM Ca^{2+}, the highest concentration used in the present work.

These relaxation experiments were analyzed using the *model-free* formalism[37] in terms of generalized order parameters (S^2) and exchange contributions (R_{ex}) to the transverse relaxation rates. The generalized order parameter S^2 represents a measure of the amplitude of the fast N–H motions and takes a value between $S^2 = 0$ (free motion) and $S^2 = 1$ (absence of motion). For [$CaCl_2$] = 1 mM, the S^2 profile is rather flat and S^2 is >0.8 for most residues, indicating that fast motion in the backbone of the core of C-HsCen2 is restricted (Fig. 5). In some regions of the protein, however, lower S^2 values of ≈ 0.6 indicate the presence of greater flexibility; in other parts, S^2 could not be determined. This is the case for the N- and C-terminal residues of the domain, for R151 (at the beginning of calcium loop IV) and for the linker between the two EF-hand motifs, particularly for L137. These dynamic effects explain the lack of structural constraints in these regions. In the presence of greater concentrations of calcium (8 mM), the S^2 profile does not change significantly, except for the termini and S122 in calcium-binding loop III.

Slow motions

The parameter R_{ex} reflects the presence of slow (microsecond to millisecond) exchange that contributes to the transverse magnetization rates $R_2(^{15}N)$ (Fig. 5). For the sample with 1 mM $CaCl_2$, a significant exchange contribution ($R_{ex} > 2.5$ s^{-1}) was observed only for residue I121. This residue is located in the small β-sheet at the interface between calcium-binding loops III and IV. The backbone of I121 establishes two H-bonds with the backbone of the
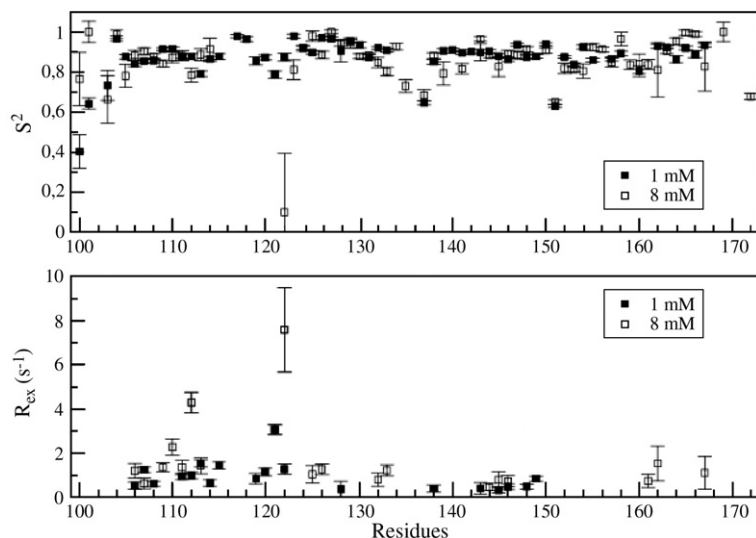
Fig. 5. Internal dynamics for the C-HsCen2/R17-hSfi1-20 complex with equimolar (1 mM, filled symbols) and excess (8 mM, open symbols) CaCl$_2$ concentrations. Order parameters S^2 (top) and R_{ex} contributions to ^{15}N transverse relaxation rates (bottom) were obtained from a model-free analysis.

facing residue V157 in loop IV. The fact that I121 presents a significant R_{ex} contribution at 1 mM CaCl$_2$ (R_{ex} could not be measured for V157) indicates that the β-sheet is not stable, probably due to the low calcium affinity of loop III (which is about 1 order of magnitude smaller than for site IV).[29] At 8 mM CaCl$_2$, residues L112 and S122 exhibited more pronounced effects, whereas the relaxation rate of I121 could not be determined because the signal decays too fast.

To obtain better insight into the enhancement of chemical exchange induced by the addition of calcium, we measured the relaxation rates of zero-quantum coherence [ZQC($C_{\pm}N_{\mp}$)] and double-quantum coherence [DQC($C_{\pm}N_{\pm}$)]. These coherences involve the backbone carbonyl ^{13}C′ of residue ($i-1$) and the amide nitrogen ^{15}N of residue (i). The difference of the relaxation rates $\Delta R = 1/2[R(DQC) - R(ZQC)]$ is determined by two contributions $R^{CSA/CSA}$ (where CSA/CSA indicates cross-correlated chemical shift anisotropy effects) and $R^{DD/DD}$ (where DD/DD indicates cross-correlated dipole–dipole effects) that depend mainly on the structure and a term $R^{CSM/CSM}$ (where CSM/CSM indicates cross-correlated isotropic chemical shift modulations) that arises from slow fluctuations of the chemical shifts (see Materials and Methods). We studied the effects of 1, 4 and 8 mM Ca^{2+} on ΔR in the C-HsCen2/R17-hSfi1-20 complex, in which only the protein is labeled. In the sample with an equimolar Ca^{2+} concentration (where only site IV is saturated), the rates ΔR could be measured for 68 of the 78 peptide bonds in C-HsCen2. The addition of Ca^{2+} resulted in a loss of peaks due to fast relaxation, such that only 63 or 58 rates could be determined in samples with 4 or 8 mM CaCl$_2$. The missing peaks mainly correspond to residues located in binding loop III. The isotropic chemical shift modulation $R^{CSM/CSM}$ contributions were deduced from ΔR, as discussed by Kateb *et al.*[36] For each sample, we first calculated the average and standard deviation over all measured rates. The values that lay outside 1.5 times the standard deviations from the average were then excluded,

leaving 59, 55 and 50 points for 1, 4 and 8 mM CaCl$_2$, respectively. Trimmed averages and standard deviations were recalculated for these restricted sets. For 1 mM CaCl$_2$, a rather flat profile along the protein sequence is obtained, with $\langle R^{CSM/CSM} \rangle = -4.5$ s^{-1} and $\sigma = 2.65$ s^{-1} (Fig. 6). For 4 mM CaCl$_2$, we found $\langle R^{CSM/CSM} \rangle = -4.6$ s^{-1}, with standard deviation $\sigma = 3.3$ s^{-1}. In the presence of an excess 8 mM CaCl$_2$, we measured $\langle R^{CSM/CSM} \rangle = -3.76$ s^{-1} and $\sigma = 4.44$ s^{-1}. These show the increasing dispersion of the $R^{CSM/CSM}$ rates with Ca^{2+} concentration. The fact that $\langle R^{CSM/CSM} \rangle$ is non-zero attests to the presence of a significant degree of conformational mobility involving most of the residues in the protein for all Ca^{2+} concentrations, which cannot be inferred from ^{15}N relaxation rates. This confirms previous observations on various proteins studied by this method.[38–40]

For the complex with 1 mM Ca^{2+}, all $R^{CSM/CSM}$ rates lie within one standard deviation of the average $\langle R^{CSM/CSM} \rangle$. In contrast, at 4 mM Ca^{2+}, contributions that significantly differ from the average were observed for residues L112, D114, D115 and G119 (Ca^{2+}-binding site III and its vicinity) and for E156 and S158 (binding site IV; see Fig. 6). Under these conditions, no relaxation rate could be measured for residues E117, T118, K120 and I121 located in binding site III due to rapid relaxation, suggesting an increased chemical exchange. Similarly, an excess of 8 mM Ca^{2+} resulted in the loss of five further peaks corresponding to residues D114, D115, D116, G119 and S122. With 8 mM Ca^{2+}, the $R^{CSM/CSM}$ values that markedly differ from the average stem from residues G155, E156, V157, S158 and E159, all of which are located in binding site IV. Furthermore, the difference of the average rates $\langle \delta R^{CSM/CSM} \rangle$ between samples with 1 and 8 mM CaCl$_2$ is only significant in loop regions in which $\langle \delta R^{CSM/CSM} \rangle = -0.18$ s^{-1} (standard deviation $\sigma = 3.88$ s^{-1}). These experiments clearly show evidence of increased exchange contributions that were not revealed by ^{15}N relaxation rates, in which only L112 and S122 revealed modified exchange rates at high calcium concentration.
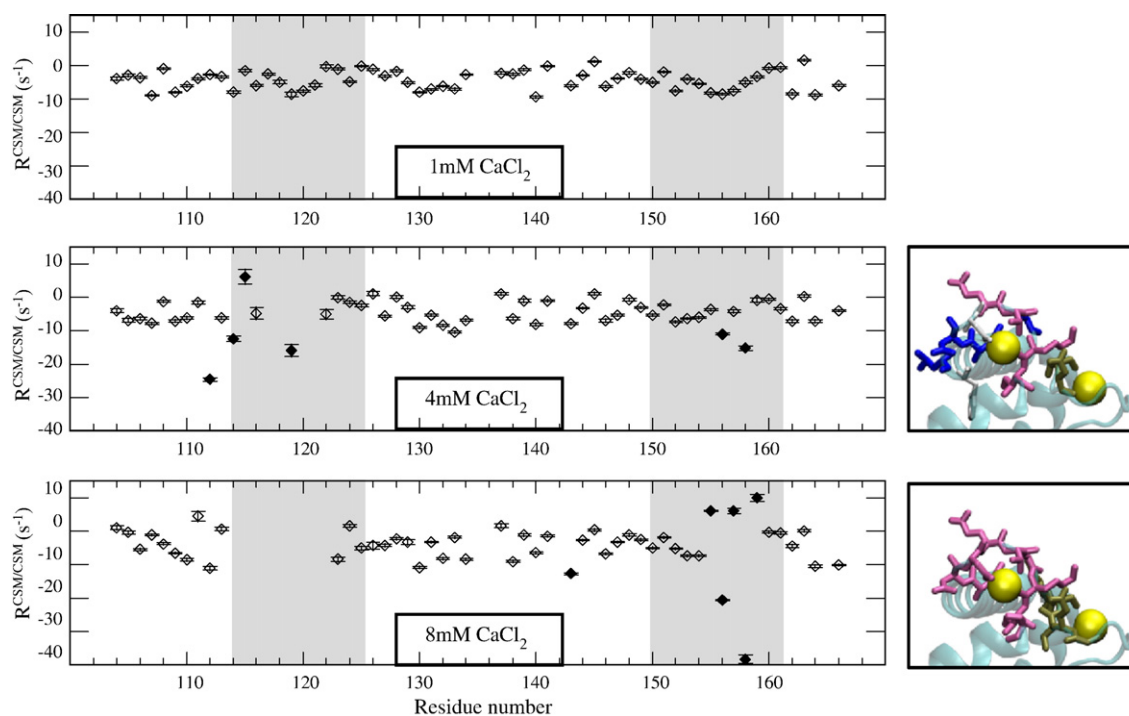
Fig. 6. Chemical shift modulation rates $R^{CSM/CSM}$ extracted from the multiple-quantum relaxation rates measured in the complex C-HsCen/R17-hSfi1-20 in samples with 1 mM CaCl$_2$ (top), 4 mM CaCl$_2$ (center) and 8 mM CaCl$_2$ (bottom). Filled symbols correspond to rates that are significantly different from the average value $\langle R^{CSM/CSM} \rangle$ (see the text for details). The gray bands indicate calcium loops III and IV. In the right panels, the calcium ions are shown as yellow spheres. Residues with $R^{CSM/CSM}$ significantly different from the average values (corresponding to filled symbols in the left panels) are in blue in calcium loop III and in tan in calcium loop IV. The residues for which the $R^{CSM/CSM}$ could not be determined are in purple. In the upper right panel, we show (in white) two residues in loop III and its close vicinity (F113 and D116) that correspond to the average $R^{CSM/CSM}$ at 4 mM CaCl$_2$.

The $R^{CSM/CSM}$ measurements performed on the complex would indicate the presence of significant slow motions in loops III and IV of C-HsCen2, the contribution to nuclear relaxation of which increases notably with the Ca^{2+} concentration. However, the dependence of these movements on calcium concentration is difficult to interpret because at higher ion concentration the binding sites should be mainly saturated and therefore less flexible. In order to account for all these dynamic observations, we hypothesized that there exists a calcium-binding subsite in loop III, in addition to the canonical one. The canonical site consists of the side chains of residues D114, D116, T118 and N125 and the backbone of K120. The subsite would consist of the side chains of D114, D115, D116, S122 and N125 and the backbone of F113 (Fig. 7). In the crystal structure of HsCen2/P17-XPC, the latter site is occupied by the amide group of N125. In our model, there would be a slow exchange between this amide group and Ca^{2+}. With a geometry less able to accommodate Ca^{2+}, the subsite would be populated only at high concentrations of CaCl$_2$. Therefore, the exchange rates R_{ex} and $R^{CSM/CSM}$ would reflect the exchange between these two positions. An NMR observation related to the resonances of the N125 amino group brings additional support to the current model. At 1 mM CaCl$_2$, the chemical shift of the nitrogen $^{15}N^{\delta 2}$ is unusually high-field shifted, in relation with the involvement

of the neighboring O$^{\delta 1}$ in Ca^{2+} coordination (Fig. S1b). With increasing Ca^{2+} concentrations, the NH$_2$ resonances of N125 broaden and eventually disappear (data not shown), indicating that the side chain of this residue (not only its backbone as observed by the $R^{CSM/CSM}$ measurements) also undergoes Ca^{2+}-induced slow motions.

As for the enhancement of $R^{CSM/CSM}$ in loop IV, the Ca^{2+} occupation of the subsite would influence the β-strand (E156, V157, S158) and its vicinity (G155, E159) in loop IV *via* S122, which is localized in loop III and faces E156 in the β-sheet. Indeed, the position of S122 should change a little but enough to induce modifications in the form of the sheet for it to interact with Ca^{2+} when it occupies the subsite.

Previous NMR experiments[36] on C-HsCen2/P17-XPC showed that with the XPC peptide, $R^{CSM/CSM}$ rates of C-HsCen2 show a smaller increase with Ca^{2+} in loop III and are not modified at all in loop IV, even at 10 mM CaCl$_2$. According to our model, this would be due to a lower probability to populate the calcium subsite in the presence of P17-XPC than of R17-hSfi1-20. A possible explanation is that F113, which interacts better with L8 of P17-XPC (see Fig. 4d and e and the structural description above), is therefore better maintained by the peptide and has less freedom to adapt to the presence of Ca^{2+} in its vicinity, making the protein less sensitive to Ca^{2+} with XPC than with hSfi1.
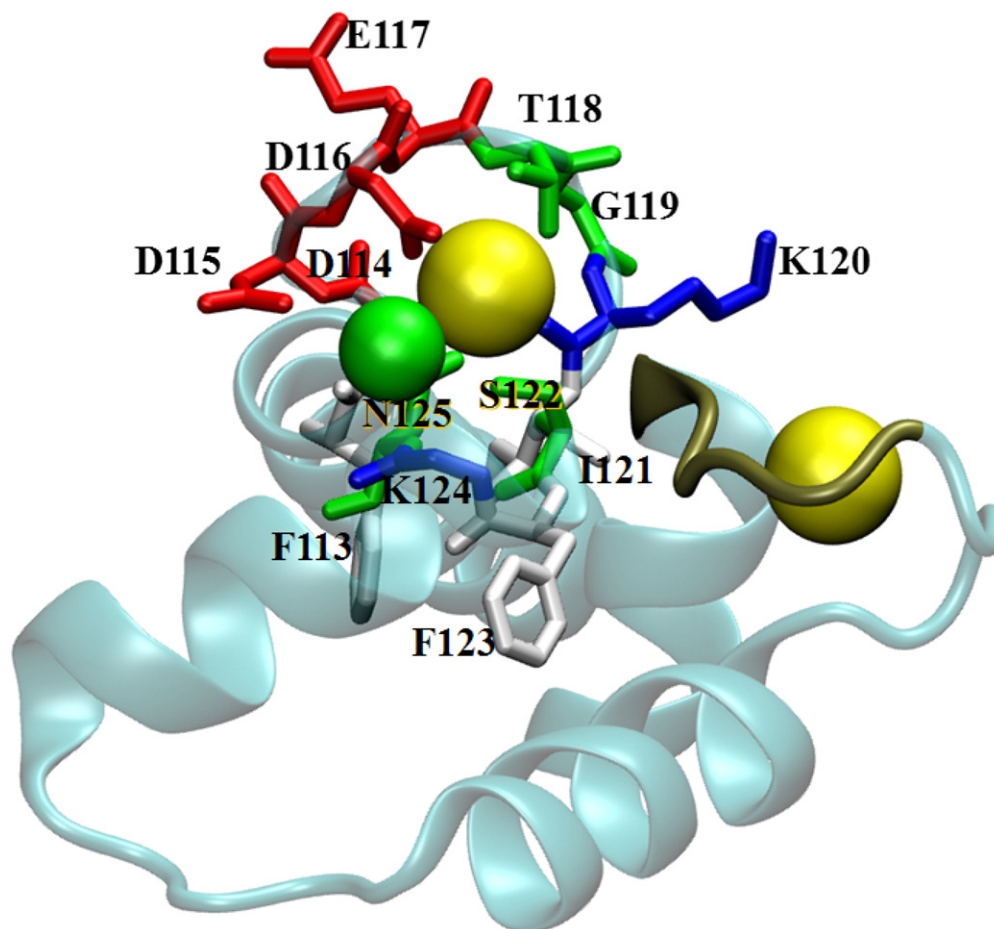
Fig. 7. Proposed alternative binding site of Ca^{2+} in loop III of HsCen2. The yellow sphere shows the canonical Ca^{2+} position, while the green sphere indicates the position of the $N^{\delta 2}$ atom of N125. Calcium ion could exchange between these two positions provided the side chain of N125 moves in concert. Side chains are color coded according to charge as in Fig. 4b. The side chain of K124 was omitted for clarity.

The existence of a secondary calcium site is made possible by the particularity of loop III, which contains three aspartate residues in its N-terminus (making the core of the subsite) and one asparagine in its C-terminus (weakening the Ca^{2+} interaction with its canonical site by the lack of the bidendate interaction with the usual Glu or Asp at this position). Examination of the sequence of the calcium-binding sites of all known EF-hand proteins showed that such a motif exists only in loop III of some centrins.

Conclusions

The study of the interactions between HsCen2 and hSfi1 repeats showed that, in contrast to the complex of yeast centrin with ScSfi1 peptide, the N-terminal domain of human centrin does not play a significant role in hSfi1 binding. The structure was therefore determined for the C-terminal domain only, complexed with the 17th repeat of hSfi1. The structure revealed the impact of the helix dipole inversion of the peptide on its affinity. This affinity is decreased (compared with the XPC peptide) because of the helix translation that induces a modification of the interactions between tryptophane W1 of hSfi1 and glutamate E148 of HsCen2 on the one hand and between leucine L8 of hSfi1 and phenylalanine F113 of HsCen2 on the other. The helix inversion also has an impact on the dynamics of Ca^{2+} binding in loop III. Indeed, the dynamics is more strongly affected by the calcium concentration for R17-hSfi1-20 than for P17-XPC, probably because of the modification of the L8/F113 interactions. To interpret these dynamics effects, we suggest that the Ca^{2+} in loop III may occupy, with a low probability, a subsite normally occupied by the side-chain amine of N125. This would be made possible by the specific structure of calcium-binding loop III in centrins. However, the loop may adjust more easily to this unusual binding mode if it is less constrained by interactions with the peptide, as for residue F113.

Materials and Methods

Synthetic peptides

Peptides corresponding to various repeats and variants of human and yeast Sfi1 (Fig. 2a) were purchased from

Hybio (Shenzhen, China) and GeneCust (Dudelange, Luxemburg). All peptides were acetylated at the N-terminal end and amidated at the C-terminal end. Purity was greater than 95%, as assessed by high-pressure liquid chromatography. In the R0-hSfi1-20 peptide, the Cys in position 10 was replaced by a Ser to avoid oxidation problems, whereas in the R9-hSfi1-20 peptide, it was not necessary to modify the Cys in position 5.

Protein production and purification

The recombinant integral HsCen2 and its N- and C-terminal domains were overproduced in *Escherichia coli* as described previously.[29,41] Purification needed three chromatographic steps, including DEAE-TSK (ion exchange), Phenyl-TSK (reversed phase) and G25 (gel filtration) columns.[42] Uniform ^{15}N and $^{15}N/^{13}C$ labeling was obtained using a minimal medium culture (M9) containing $^{15}NH_4Cl$ and ^{13}C-glucose as the sole sources of nitrogen and carbon, respectively. The induction step (with IPTG of 0.1 mM) was prolonged to 18 h in these cases.

Isothermal titration calorimetry

The thermodynamic parameters of molecular interactions between centrin and target peptides were investigated by ITC using a MicroCal MCS instrument (MicroCal Inc., Northampton, MA). The protein and the peptide were equilibrated in the same buffer containing 50 mM Mops at pH 7.4, 100 mM NaCl and 1 mM $CaCl_2$ or 2 mM ethylenediaminetetraacetic acid (to eliminate potential traces of calcium). The 15–20 μM centrin was titrated by injecting the peptide (which was 10 times more concentrated) with automatic injections of 8–10 μl at 303 K. The first injection of 2 μl was ignored in the final data analysis. Integration of the peaks for each injection and baseline corrections were carried out using an Origin-based software provided by the manufacturer. Fitting the data to an interaction model allows one to obtain the stoichiometry (n), the equilibrium binding constant (K_a) and the enthalpy of complex formation (ΔH). All experiments were repeated twice and gave similar results. Control experiments consisting of injections of the peptide solution into the buffer were performed to evaluate the heat of dilution.

NMR spectroscopy

NMR samples at 1.2 mM concentration, pH 6.7, were obtained by dissolving the lyophilized protein in a buffer containing 20 mM deuterated Tris–DCl, 100–200 mM NaCl and 1.5 mM $CaCl_2$ in 93% ^1H_2O/7% ^2H_2O or in 100% ^2H_2O. The unlabeled R17-hSfi1-20 peptide was added in slight molar excess. Two-dimensional homonuclear experiments, as well as double- and triple-resonance [HSQC, NOESY (NOE spectroscopy)-HSQC, TOCSY (total correlated spectroscopy)-HSQC, HNCA, HN(CO)CA and HCCH-TOCSY] experiments,[43,44] were performed on Varian Unity 500 and Bruker Avance 800 spectrometers at 308 K. Proton chemical shifts in parts per million were referenced relative to internal DSS (2,2-dimethyl-2-silapentane-5-sulfonate), while ^{15}N and ^{13}C references were determined indirectly relative to DSS using frequency ratios.[45] NMR data were processed and analyzed using the Felix software (Accelrys, San Diego, CA) running on Silicon Graphics workstations. For the three-dimensional ^{15}N TOCSY-HSQC and NOESY-HSQC spectra, the data were extrapolated by linear prediction in the indirect

dimensions, zero-filled and multiplied by π/4-shifted sine-bell functions before Fourier transformation. The three-dimensional (^1H, ^{15}N) spectra were acquired with 7000- and 1500 -Hz spectral widths in the ^1H and ^{15}N dimensions, respectively. One hundred twenty-eight complex points were collected in the t_1 dimension (^1H), 32 complex points were collected in the t_2 (^{15}N) dimension and 2048 complex points were collected in the t_3 dimension.

Structure calculation

NOE restraints were classified in three classes: strong (1.8–3.0 Å), medium (3.0–3.8 Å) and weak (3.8–5.0 Å). Moreover, the NOE restraints in secondary structure elements were adjusted to fall into standard ranges for helical segments [i.e., $d_{\alpha N}(i,i+1)$=3.3–3.7 Å, $d_{\alpha N}(i,i+2)$= 4.2–4.6 Å, $d_{NN}(i,i+1)$=2.6–3.0 Å and $d_{NN}(i,i+2)$=4.0–4.4 Å] and for β-strand structures [$d_{\alpha N}(i,i+1)$=2.0–2.4 Å]. A number of hydrogen bonds involved in secondary structures were also included as distance restraints by using upper and lower distances of 2.2 and 1.8 Å, respectively, for (H, O) pairs and 3.3 and 2.7 Å, respectively, for (N, O) pairs. For α-helices and β-strands, dihedral angles Φ_H=−60° (±30°), Ψ_H=−30° (±40°) and Φ_S=−130° (±30°), Ψ_S=145° (±35°), respectively, were imposed. The structure determination was performed using 1064 intraprotein NOE restraints and 71 intermolecular distance restraints (Table 2). An additional set of 84 restraints was derived from hydrogen-bond identification, and 120 dihedral angle restraints resulted from the secondary structure determination. The calculation of the structures was carried out using the Discover software and the CVFF force field (Accelrys, San Diego, CA) running on an SGI workstation. Starting from an initial extended conformation, 200 structures were generated using simulated annealing, including a 30-ps high-temperature phase (at 1000 K), followed by a cooling phase (down to 300 K) of 8 ps and final energy minimization. A force constant of 20 kcal mol^{-1} Å^{-2} was used for NOE distance restraints. Restraints of dihedral angles Φ and Ψ used a force constant of 30 kcal mol^{-1} rad^{-2}. The quality of the 15 final structures, selected according to the potential energy and the compatibility with experimental restraints, was analyzed using the InsightII and PROCHECK-NMR programs.

Nuclear relaxation

All dynamics experiments were performed at 308 K on a 600-MHz Bruker Avance spectrometer equipped with triple-axis gradients on samples dissolved in 90% H_2O/10% D_2O. Spectra were processed using the NMRPipe/NMRDraw package. A squared cosine apodization window was used, and the digital resolution was improved by using zero filling in both dimensions. Peaks were fitted to Gaussian line shapes with the least-squares routine.

Fast motions occurring on the picosecond-to-nanosecond timescale were investigated through measurements of amide R_1(^{15}N) and R_2(^{15}N) relaxation rates and heteronuclear $^{15}N\{^1H\}$ nuclear Overhauser effects. The R_1 and R_2 experiments were acquired in an interleaved manner.[46] For longitudinal R_1 relaxation rates, delays of 5, 50, 100, 150, 250, 300, 370, 500 and 650 ms were used, and R_2 relaxation rate measurements were performed with relaxation intervals of 2, 20, 40, 60, 80, 100, 120 and 148 ms. The recovery delay between acquisitions was 1.8 s, and 16 transients were acquired for each of the 256 t_1 time increments. Water signal suppression was achieved using the WATERGATE

technique.[47] For both experiments, intensities were fitted to a single exponential with a home-written script using the Scilab software to extract the corresponding relaxation rates. Heteronuclear NOE experiments were performed using 512 (complex) points in the ^{1}H dimension, with 8 transients for each t_1 increment and a recovery delay of 12 s. The analysis of the backbone ^{15}N relaxation data was then performed using the model-free approach as implemented in the TENSOR2 software.[48]

Slow processes on a microsecond-to-millisecond time-scale were investigated by measuring multiple-quantum relaxation rates ZQC($C_\pm N_\mp$) and DQC($C_\pm N_\pm$) involving the backbone carbonyl ^{13}C′ of residue $(i-1)$ and the amide nitrogen ^{15}N of residue (i). As shown elsewhere,[36,40] the difference between the ZQC and DQC relaxation rates $\Delta R = 1/2[R(\text{DQC}) - R(\text{ZQC})]$ is determined by contributions from cross-correlated dipole–dipole (DD/DD) and chemical shift anisotropy (CSA/CSA) effects, as well as isotropic chemical shift modulations (CSM/CSM):

$$\Delta R = R^{\text{CSM/CSM}} + R^{\text{DD/DD}} + R^{\text{CSA/CSA}}$$

The last two terms can be estimated from the molecular structure and the knowledge of the ^{15}N and ^{13}C isotropic chemical shifts.[36,40,49] However, residues belonging to the N- and C-termini of the protein, which are very flexible, were not taken into account in the analysis as their $R^{\text{DD/DD}}$ and $R^{\text{CSA/CSA}}$ contributions to the multiple-quantum rates were difficult to estimate. Measurements of ZQC($C_\pm N_\mp$) and DQC($C_\pm N_\pm$) rates were performed using a pulse sequence derived from an HNCO experiment,[40] where the ^{13}C evolution period was replaced by a multiple-quantum coherence relaxation delay τ. Coherences $2N_x C_x$ and $2N_y C_y$ were detected in an interleaved manner. To improve the accuracy, we repeated the experiments with three intervals, $\tau = 20$, 40 and 50 ms, each obtained with 64 scans. The differential line broadening ΔR was obtained from the ratio $\langle 2N_x C_x \rangle / \langle 2N_y C_y \rangle = \tan h(\Delta R \tau)$.

Accession numbers

The atomic coordinates of a set of 15 structures corresponding to the complex C-HsCen2/R17-hSfi1-20 have been deposited in the PDB‡ under accession code 2K2I. The ^{1}H, ^{15}N and ^{13}C chemical shift values of this complex have been deposited in BioMagResBank§ under accession number 15755.

‡ http://www.rcsb.org
§ http://www.bmrb.wisc.edu

Supplementary Data

Supplementary data associated with this article can be found, in the online version, at doi:10.1016/j.jmb.2009.10.041

References

1. Schiebel, E. & Bornens, M. (1995). In search of a function for centrins. *Trends Cell Biol.* **5**, 197–201.
2. Salisbury, J. L. (1995). Centrin, centrosomes and mitotic spindle poles. *Curr. Opin. Cell Biol.* **7**, 39–45.
3. Salisbury, J. L., Baron, A., Surek, B. & Melkonian, M. (1984). Striated flagellar roots: isolation and partial characterization of a calcium-modulated contractile organelle. *J. Cell Biol.* **99**, 962–970.
4. Huang, B., Mengersen, A. & Lee, V. D. (1988). Molecular cloning of cDNA for caltractin, a basal body-associated Ca^{2+}-binding protein: homology in its protein sequence with calmodulin and the yeast CDC31 gene product. *J. Cell Biol.* **107**, 133–140.
5. Sanders, M. A. & Salisbury, J. L. (1994). Centrin plays an essential role in microtubule severing during flagellar excision in *Chlamydomonas reinhardtii*. *J. Cell Biol.* **124**, 795–805.
6. Geimer, S. & Melkonian, M. (2005). Centrin scaffold in *Chlamydomonas reinhardtii* revealed by immunoelectron microscopy. *Eukaryotic Cell*, **4**, 1253–1263.
7. Zhu, J.-K., Bressan, R. & Hasegawa, P. (1992). An *Atriplex nummularia* cDNA with sequence relatedness to the algal caltractin gene. *Plant Physiol.* **99**, 1734–1735.
8. Baum, P., Furlong, C. & Byers, B. (1986). Yeast gene required for spindle pole body duplication: homology of its product with Ca^{2+}-binding proteins. *Proc. Natl Acad. Sci. USA*, **83**, 5512–5516.
9. Wolfrum, U. (1992). Cytoskeletal elements in arthropod sensilla and mammalian photoreceptors. *Biol. Cell*, **76**, 373–381.
10. Lee, V. D. & Huang, B. (1993). Molecular cloning and centrosomal localization of human caltractin. *Proc. Natl Acad. Sci. USA*, **90**, 11039–11043.
11. Errabolu, R., Sanders, M. A. & Salisbury, J. L. (1994). Cloning of a cDNA encoding human centrin, an EF-hand protein of centrosomes and mitotic spindle poles. *J. Cell Sci.* **107**, 9–16.
12. Wolfrum, U., Giesl, A. & Pulvermüller, A. (2002). Centrins, a novel group of Ca^{2+}-binding proteins in vertebrate photoreceptor cells. In *Photoreceptors and Calcium* (Baehr, W. & Palczewski, K., eds), pp. 155–178, Kluwer Academic, New York, NY.
13. Marshall, W. F., Vucica, Y. & Rosenbaum, J. L. (2001). Kinetics and regulation of *de novo* centriole assembly: implications for the mechanism of centriole duplication. *Curr. Biol.* **11**, 308–317.
14. Salisbury, J. L., Suino, K. M., Busby, R. & Springett, M. (2002). Centrin-2 is required for centriole duplication in mammalian cells. *Curr. Biol.* **12**, 1287–1292.
15. Paoletti, A., Bordes, N., Haddad, R., Schwartz, C. L., Chang, F. & Bornens, M. (2003). Fission yeast cdc31p is a component of the half-bridge and controls SPB duplication. *Mol. Biol. Cell*, **14**, 2793–2808.
16. Koblenz, B., Schoppmeier, J., Grunow, A. & Lechtreck, K.-F. (2003). Centrin deficiency in *Chlamydomonas* causes defects in basal body replication, segregation and maturation. *J. Cell Sci.* **116**, 2635–2646.

17. Selvapandiyan, A., Debrabant, A., Duncan, R., Muller, J., Salotra, P., Sreenivas, G. *et al.* (2004). Centrin gene disruption impairs stage-specific basal body duplication and cell cycle progression in *Leishmania. J. Biol. Chem.* **279**, 25703–35710.

18. Araki, M., Masutani, C., Takemura, M., Uchida, A., Sugasawa, K., Kondoh, J. *et al.* (2001). Centrosome protein centrin 2/caltractin 1 is part of the xeroderma pigmentosum group C complex that initiates global genome nucleotide excision repair. *J. Biol. Chem.* **276**, 18665–18672.

19. Giessl, A., Pulvermuller, A., Trojan, P., Park, J. H., Choe, H.-W., Ernst, O. P. *et al.* (2004). Differential expression and interaction with the visual G-protein transducin of centrin isoforms in mammalian photoreceptor cells. *J. Biol. Chem.* **279**, 51472–51481.

20. Gonda, K., Yoshida, A., Oami, K. & Takahashi, M. (2004). Centrin is essential for the activity of the ciliary reversal-coupled voltage-gated Ca^{2+} channels. *Biochem. Biophys. Res. Commun.* **323**, 891–897.

21. Guerra, C., Wada, Y., Leick, V., Bell, A. & Satir, P. (2003). Cloning, localization and axonemal function of *Tetrahymena* centrin. *Mol. Biol. Cell*, **14**, 251–261.

22. Fischer, T., Rodriguez-Navarro, S., Pereira, G., Racz, A., Schiebel, E. & Hurt, E. (2004). Yeast centrin Cdc31 is linked to the nuclear mRNA export machinery. *Nat. Cell Biol.* **6**, 840–848.

23. Kilmartin, J. V. (2003). Sfi1p has conserved centrin-binding sites and an essential function in budding yeast spindle body duplication. *J. Cell Biol.* **162**, 1211–1221.

24. Martinez-Sanz, J., Yang, A., Blouquit, Y., Duchambon, P., Assairi, L. & Craescu, C. T. (2006). Binding of human centrin 2 to the centrosomal protein hSfi1. *FEBS J.* **273**, 4504–4515.

25. Thompson, J. R., Ryan, Z. C., Salisbury, J. L. & Kumar, R. (2006). The structure of the human centrin 2–xeroderma pigmentosum group C protein complex. *J. Biol. Chem.* **281**, 18746–18752.

26. Charbonnier, J.-B., Renaud, E., Miron, S., Le Du, M. H., Blouquit, Y., Duchambon, P. *et al.* (2007). Structural, thermodynamic and cellular characterization of human centrin 2 interaction with xeroderma pigmentosum group C protein. *J. Mol. Biol.* **373**, 1032–1046.

27. Li, S., Sandercock, A. M., Conduit, P., Robinson, C. V., Williams, R. L. & Kilmartin, J. V. (2006). Structural role of Sfi1p–centrin filaments in budding yeast spindle pole duplication. *J. Cell Biol.* **173**, 867–877.

28. Veeraraghavan, S., Fagan, P. A., Hu, H., Lee, V., Harper, J. F., Bessie, H. & Chazin, W. J. (2002). Structural independence of the two EF-hand domains of caltractin. *J. Biol. Chem.* **277**, 28564–28571.

29. Matei, E., Miron, S., Blouquit, Y., Duchambon, P., Durussel, I., Cox, J. A. & Craescu, C. T. (2003). The C-terminal half of human centrin 2 behaves like a regulatory EF-hand domain. *Biochemistry*, **42**, 1439–1450.

30. Chattopadhyaya, R., Meador, W. E., Means, A. R. & Quiocho, F. A. (1992). Calmodulin structure refined at 1.7 Å resolution. *J. Mol. Biol.* **228**, 1177–1192.

31. Popescu, A., Miron, S., Blouquit, Y., Duchambon, P. & Craescu, C. T. (2003). Xeroderma pigmentosum group C protein possesses a high affinity binding site for human centrin 2 and calmodulin. *J. Biol. Chem.* **278**, 40252–40261.

32. Cox, J. A., Durussel, I., Firanescu, C., Blouquit, Y., Duchambon, P. & Craescu, C. T. (2005). Calcium and magnesium binding to human centrin 3 and interaction with target peptides. *Biochemistry*, **44**, 840–850.

33. Carafoli, E. (2003). The calcium-signalling saga: tap water and protein crystals. *Nat. Rev. Mol. Cell Biol.* **4**, 326–332.

34. Yang, A., Miron, S., Mouawad, L., Duchambon, P., Blouquit, Y. & Craescu, C. T. (2006). Flexibility and plasticity of human centrin 2 binding to the protein XPC from nuclear excision repair. *Biochemistry*, **45**, 3653–3663.

35. Gemmecker, G., Olejniczak, E. T. & Fesik, S. W. (1992). An improved method for selectively observing protons attached to ^{12}C in the presence of ^1H–^{13}C spin pairs. *J. Magn. Reson.* **96**, 199.

36. Kateb, F., Abergel, D., Blouquit, Y., Duchambon, P., Craescu, C. T. & Bodenhausen, G. (2006). Slow backbone dynamics of the C-terminal fragment of human centrin 2 in complex with a target peptide probed by cross-correlated relaxation in multiple-quantum NMR spectroscopy. *Biochemistry*, **45**, 15011–15019.

37. Lipari, G. & Szabo, A. (1982). Model-free approach to the interpretation of nuclear magnetic resonance relaxation in macromolecules: 1. Theory and range of validity. *J. Am. Chem. Soc.* **104**, 4546–4559.

38. Wist, J., Frueh, D., Tolman, J. R. & Bodenhausen, G. (2003). Triple quantum decoherence under multiple refocusing: slow correlated chemical shift modulations of C′ and N nuclei. *J. Biomol. NMR*, **28**, 263–272.

39. Wist, J., Perazzolo, C. & Bodenhausen, G. (2005). Slow motions in nondeuterated proteins: concerted chemical shift modulations of backbone nuclei. *Appl. Magn. Reson.* **29**, 251–259.

40. Perazzolo, C., Wist, J., Loth, K., Poggi, L., Homans, S. & Bodenhausen, G. (2005). Effects of protein–pheromone complexation on correlated chemical shift modulations. *J. Biomol. NMR*, **33**, 233–242.

41. Durussel, I., Blouquit, Y., Middendorp, S., Craescu, C.T. & Cox, J. A. (2000). Cation- and peptide-binding properties of human centrin 2. *FEBS Lett.* **472**, 208–212.

42. Yang, A., Miron, S., Duchambon, P., Assairi, L., Blouquit, Y. & Craescu, C. T. (2006). The N-terminal domain of human centrin 2 has a closed structure, binds calcium with a very low affinity, and plays a role in the protein self-assembly. *Biochemistry*, **45**, 880–889.

43. Wüthrich, K. (1986). *NMR of Proteins and Nucleic Acids.* Wiley, New York, NY.

44. Cavanagh, J., Fairbrother, W. J., Palmer, A. G., III & Skelton, N. J. (1996). *Protein NMR Spectroscopy. Principles and Practice.* Academic Press, San Diego, CA.

45. Wishart, D. S., Bigam, C. G., Yao, J., Abildgaard, F., Dyson, H. J., Oldfield, E. *et al.* (1995). ^1H, ^{13}C, and ^{15}N chemical shift referencing in biomolecular NMR. *J. Biomol. NMR*, **6**, 135–140.

46. Farrow, N. A., Muhandiram, R., Singer, A. U., Pascal, S. M., Kay, C. M., Gish, G. *et al.* (1994). Backbone dynamics of a free and phosphopeptide-complexed Src homology 2 domain studied by ^{15}N NMR relaxation. *Biochemistry*, **33**, 5984–6003.

47. Piotto, M., Saudek, V. & Sklenar, V. (1992). Gradient-tailored excitation for single-quantum NMR spectroscopy of aqueous solutions. *J. Biomol. NMR*, **2**, 661–665.

48. Dosset, P., Hus, J.-C., Blackledge, M. & Marion, D. (2000). Efficient analysis of macromolecular rotational diffusion from heteronuclear relaxation data. *J. Biomol. NMR*, **16**, 23–28.

49. Loth, K., Pelupessy, P. & Bodenhausen, G. (2005). Chemical shift anisotropy tensors of carbonyl, nitrogen and amide proton nuclei in proteins through cross-correlated relaxation in NMR spectroscopy. *J. Am. Chem. Soc.* **127**, 6062–6068.